

Chapter 13

Removal of Uranium from Flowback Water of Hydraulic Fracturing Processes in Unconventional Reservoirs Using Phosphorus- and Nitrogen-Functionalized Activated Carbons



Karol Z. Acosta, Mauricio Holguín, Mónica M. Lozano, Francisco Carrasco-Marín, Raúl Ocampo, Agustín F. Pérez-Cadenas, Camilo A. Franco, and Farid B. Cortés

13.1 Introduction

Gas unconventional reservoirs are currently considered as viable sources of energy for different countries to ensure their requirements and increase the reserves to consolidate energy self-sufficiency [1, 2]. Thus, the production of unconventional oil and gas has increased continuously. For example, in 2015, the annual production of unconventional oil and gas amounted to 30 billion BOPD and $9.273 \times 10^8 \text{ Nm}^3$ [3], respectively, mainly due to the hydraulic fracturing (HF). Hydraulic fracturing is a technique commonly used for the oil and gas exploitation in reservoirs of ultralow permeability rocks such as tight, shale, and coal beds. This technique uses water-based fluids composed of surfactants, polymer, clay stabilizers, biocide, and sand that are injected at high pressures into the formation [4]. This process creates new

K. Z. Acosta · M. Holguín · M. M. Lozano · C. A. Franco (✉) · F. B. Cortés (✉)
Grupo de Investigación en Fenómenos de Superficie–Michael Polanyi, Facultad de Minas,
Universidad Nacional de Colombia – Sede Medellín, Medellín, Colombia
e-mail: kzapata@unal.edu.co; jmholguinas@unal.edu.co; caafancoar@unal.edu.co;
fbcortes@unal.edu.co

F. Carrasco-Marín · A. F. Pérez-Cadenas
Grupo de Investigación en Materiales del Carbón, Facultad de Ciencias, Universidad de
Granada, Granada, Spain
e-mail: fmarin@ugr.es; afperez@ugr.es

R. Ocampo
Centro de Investigaciones y Estudios de Posgrado, Facultad de Ciencias Químicas,
Universidad Autónoma de San Luis de Potosí, San Luis de Potosí, Mexico
e-mail: raul.ocampo@uaslp.mx

fractures in the formation, favoring the well productivity due to the increased connectivity of existing pores and fractures, and hence increases the permeability to conduct the fluids into the well [5]. Nevertheless, the rock associated to these reservoirs has different radioactive elements such as thorium (Th) and uranium (U) [6], which are known as naturally occurring radioactive materials (NORM) [7]. Terrestrial NORM typically found in geological formations consists of isotopes from the uranium-238 decay series, thorium-232 decay series, and potassium-40. In many cases it is the decay products of the uranium and thorium decay chain that present a larger problem to the environment (e.g., Radon-228). Accordingly, significant amounts of produced waters are generated during the exploitation and fracturing processes named production water flowback, which carry with it sand, chemical, organic compounds, radioactive elements (depending on the geochemical of the formation), among others [4, 7]. The NORM are well-documented contaminants of oil and gas wastes [7]. However, to the best of our knowledge, there are no studies reported in the scientific literature about NORM removal from the water production in HF process in unconventional reservoirs. Some authors report the adsorption of uranyl (VI) ions in aqueous solutions by magnetic polyethyleneimine-modified activated coal [8], NORM adsorption by a batch of insolubilized humic acid [9], biosorption removal of Th(IV) by *Aspergillus niger* [10], and others that include adsorption with other materials like zeolite, two-dimensional MXene material, and resins [11, 12]. Therefore, the main objective of this work is to develop activated carbons (AC) from olive stones with unique chemical surface characteristics for uranium (U) removal. For this proposal, carbon surfaces have been modified by doping with different heteroatoms of nitrogen, phosphorus, and phosphorus/nitrogen. The adsorption studies have been focused on uranyl acetate aqueous solutions. Moreover, the effects of the chemical nature of the adsorbent, adsorbent/adsorbate ratio, and salinity were evaluated based on the fluid-surface interactions. Besides, the obtained isotherms were fitted with a mathematical model for explaining the phenomenological behavior. Finally, a reuse test was designed based on the desorption/adsorption data for understanding the perdurability of the synthesized materials.

13.2 Materials and Methods

13.2.1 Materials

Olive stones (agro-industrial waste) were selected as raw material for activated carbon production. These were crushed and sieved to 1.0–2.0 mm size and subsequently dried at 90 °C until constant weight. Phosphoric acid (reagent grade $\geq 80\%$, Sigma-Aldrich, St. Louis, MO, USA) was employed for the chemical activation of the raw material before carbonization. Melamine (99%, Sigma Aldrich, St. Louis, MO, USA), phosphoric acid, and ammonium phosphate (reagent grade $\geq 98\%$, Sigma Aldrich, St. Louis, MO, USA) were used for the functionalization of the

material surface. Distilled water was used for the washing protocol. On the other hand, a uranyl acetate was used as a precursor of the uranyl ion (reagent grade $\geq 98\%$, Sigma Aldrich, St. Louis, MO, USA).

13.2.2 Methods

13.2.2.1 Preparation of Activated Carbons

Activated carbons (ACs) were produced by chemical activation of olive stones with the phosphoric acid solution following the process before described by Moreno-Castilla et al. [13]. Thus, 100 g of olive stones were mixed with the phosphoric acid solution in a mass ratio of 1:2. The mixture was macerated and dried using an IR lamp for 20 h. It was then carbonized in a tubular furnace (Heraeus, Hanau, Germany) by heating at $10\text{ }^{\circ}\text{C}/\text{min}$ up to $840\text{ }^{\circ}\text{C}$. A soaking time of 2 h under a nitrogen flow of $300\text{ cm}^3/\text{min}$ was used. The material obtained was treated with distilled water until $\text{pH} = 7$.

13.2.2.2 Modification of Activated Carbons

After the AC material was dried at $100\text{ }^{\circ}\text{C}$ for 24 h, an incipient impregnation process was used for surface modifications [14]. In this sense, an appropriate quantity of functionalizing agents such as melamine, phosphoric acid, and ammonium phosphate was used to dope the carbon surface with heteroatoms such as N (AC-N), P (AC-P), or N and P (AC-NP) in the AC sample, respectively. For this proposal, the solutions with the heteroatoms (P, N, and N and P) were prepared based on the solubility limit in water and/or ethanol [15]. Then, these solutions were gradually dropped on AC material. After the impregnation, the materials were dried using an IR lamp for 20 h, and finally, they were heated at $700\text{ }^{\circ}\text{C}$ under a nitrogen.

13.2.2.3 Characterization of Activated Carbons

Scanning electron microscopy (SEM) analysis was used for studying the morphology of the materials using a GEMINI-1530 microscope (Berlin, Germany). Textural properties were calculated from sorption isotherms of N_2 using a Quadrasorb SI instrument (Florida, USA). Previously, the carbons were degassed overnight at $110\text{ }^{\circ}\text{C}$. The Brunauer–Emmett–Teller (BET) equation was fitted to isotherms to estimate the surface area (S_{BET}), while the Dubinin–Radushkevich (DR) model was used to calculate the micropore properties (micropore volume, V_{mic} , and micropore mean size, L_{mic}) [16]. Mercury porosimetry was developed to obtain the macropore volume V_{macro} (pore size from 50 to 10,000 nm) and mesopore, L_{meso} , and macropore width (L_{macro}) by using an AutoPore IV 9510 instrument up to a pressure of

2000 kg cm⁻² (Georgia, USA). Pore size distributions (PSD) were calculated by the application of QSDFT to N₂ adsorption isotherms and mercury porosimetry results. Total pore volume, V_T , was calculated from the whole PSD, and mesopore volume, V_{meso} , was calculated by the integration between 2 and 50 nm. The carbon chemical properties were obtained by X-ray photoelectron spectroscopy analysis (XPS) and by determining the pH_{IEP} [17].

13.2.2.4 Material Selection

In order to determine the most efficient materials during U removal, adsorption tests were carried out according to the method previously reported by Khalili et al. [12]. Adsorption assays were carried out in aqueous solutions, in the absence of salts and using a ratio of 10:1 adsorbent/adsorbate and 500 mg/L of uranyl in solution. The adsorptive couple is contacted during 24 h at 300 rpm later, they are separated by centrifugation (4000 rpm), and the residual uranyl content in the supernatant was determined by using a spectrofluorometer with $\lambda_{\text{Exc.}}=369$ nm, $\lambda_{\text{Emi.}}=510$, Slit exc. = 10 nm, and Slit emi. = 10 nm (Thermo Scientific, Waltham, MA, USA).

13.2.2.5 Adsorption Isotherms

Uranyl adsorption isotherms were developed on the materials that turned out to be more efficient. For this, a solution containing 1000 mg/L of uranyl acetate (U) in deionized water was prepared and subsequently diluted at concentrations between 10 and 500 mg/L in the different systems (varying the amount of ACs materials and varying salinity) at pH 6.3. The residual concentration of U during the adsorption was determined by using spectrofluorometer (Thermo Scientific, Waltham, MA, USA) to the conditions previously described. The time for reaching the adsorption equilibrium was around 4 hours. The amounts adsorbed in units of milligram of uranyl per gram mass of materials were estimated according to Eq. (13.1) according to the method described by Franco et al. [18]:

$$N_{\text{ads}} = \frac{(C_0 - C_e)V}{W} \quad (13.1)$$

Where C_0 (mg/L) is the initial uranyl concentration while C_e (mg/L) is the uranyl equilibrium concentrations; V (L) is the volume of the uranyl solution, and W (g) is the mass of carbons used to essay. The concentration of uranyl residual in the supernatant was determined by fluorescence as described above.

13.2.2.6 Effect of Adsorbent/Adsorbate Ratio on Adsorption Efficiency of Uranyl

For this, different amounts of ACs materials were employed (100 mg per 20 ml of uranyl solution (a ratio of 5:1), 200 mg per 20 mL of solution (10:1), and 400 mg per 20 ml of solution (20:1)), and the other conditions for the adsorption were maintained constant. The isotherms were estimated as explained above.

13.2.2.7 Effect of Salinity on Adsorption Efficiency of Uranyl

For this, three salt concentrations using KCl were prepared (1% w/v, 3% w/v, and 5% w/v; the salinities were chosen considering the average hardness of the flowback water), and the other conditions were maintained constant (adsorbent/adsorbate ratio 10:1 and pH 6.3). Then, isotherms were estimated, as explained above.

13.2.2.8 Reuse Process

The desorption test of using basic solutions was carried out in order to evaluate the capacity of the material in reuse processes. For this, the composites AC material-uranyl were left in a NaOH solution at pH of 12.0. After 24 h, the content of uranyl in the medium was monitored by fluorescence using a new calibration curve. Subsequently, the materials were used in resorption tests. For this, 200 mg of desorbed materials were added to 10 ml of an aqueous solution of uranyl to 500 mg/L (pH = 6.3), then the mixture was stirred at 300 rpm during 4 h, and the content of uranyl in the solutions was again measured; a total of 30 adsorption-re-adsorption cycles were carried out.

13.2.2.9 Solid-Liquid Equilibrium (BET) Model

The BET model has been extensively used to fit sorption isotherm experimental data [19]. This model describes mainly the multilayer adsorption phenomena for liquid-solid systems [20–23]. The model is presented below:

$$q = q_{\max} \frac{K_S C_E}{(1 - K_L C_E)(1 - K_L C_E + K_S C_E)}$$

where q is the amount of uranyl (mg/g) adsorbed at equilibrium, q_{\max} is the maximum adsorption capacity (mg/g), C_E is the equilibrium concentration of uranyl in the aqueous phase (mg/L), and K_S (L/mg) and K_L (L/mg) are the equilibrium constants of adsorption for the first layer and the upper layers, respectively.

13.3 Results

13.3.1 Material Characterization

AC morphologies were analyzed by SEM; illustrative images are shown in Fig. 13.1. AC samples are three-dimensional networks of amorphous particles in a micrometric regime, arranged randomly, and with spaces between the primary particles, which define their porosity, which is essential for physisorption phenomena. Other studies have described this type of arrangement [24, 25].

The N_2 sorption isotherms of AC materials are presented in Fig. 13.2. Carbons show type I–IV hybrid isotherms with a H4 hysteresis loop according to IUPAC (International Union of Pure and Applied Chemistry) [26], and these results are characteristic of microporous-mesoporous hybrid materials with narrow slit-like pores. The slight slope at low relative pressures less than 0.1 is evidence of the development of the monolayer. After that, the curve is pronounced indicating the beginning of the multilayer fission, which corresponds to the filling of mesopores. Other studies have revealed the ability of phosphoric acid to increase the micro- and mesoporous space, causing the collapse of macropores [25, 27, 28].

The textural properties of materials derived from the isotherms are summarized in Table 13.1. All samples (AC materials) were microporous-mesoporous hybrid; V_{micro} and V_{meso} represented, each one, the 40% of V_T . Functionalized materials exhibited V_T slightly lower than the AC sample (control), which is expected, considering that the heteroatoms block the pore by deposition in the micro- and mesoporous spaces [27]. However, the modification with phosphoric acid (P) had a dual activating consequence, increasing total porous volume.

The pore size distributions (PSD) of the AC materials are shown in Fig. 13.3. The results attained by the coupling of nitrogen isotherms and mercury porosimetry confirm that carbon materials are microporous–mesoporous materials; V_{macro} represents less than 20% of V_T in all cases. All distributions showed bimodal behaviors;

Fig. 13.1 The microstructure of the activated carbon without functionalization (AC) sample obtained by SEM analysis

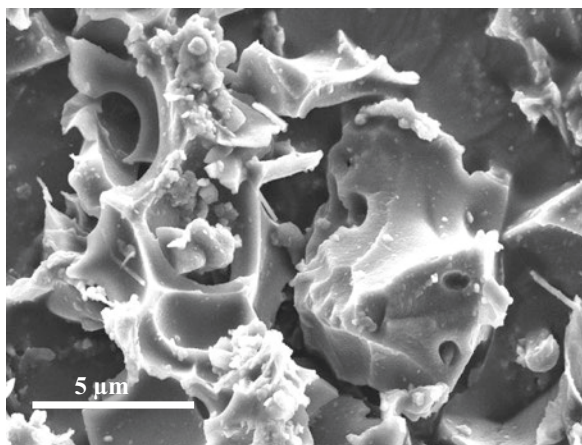


Fig. 13.2 N₂-Isotherms at –196 °C for ●, activated carbon without functionalization (AC); ◆, activated carbon functionalized with melamine (AC-N); ▲, activated carbon functionalized with phosphoric acid (AC-P); and ■, activated carbon functionalized with ammonium phosphate (AC-NP). Adsorption (open symbols); desorption (closed symbols)

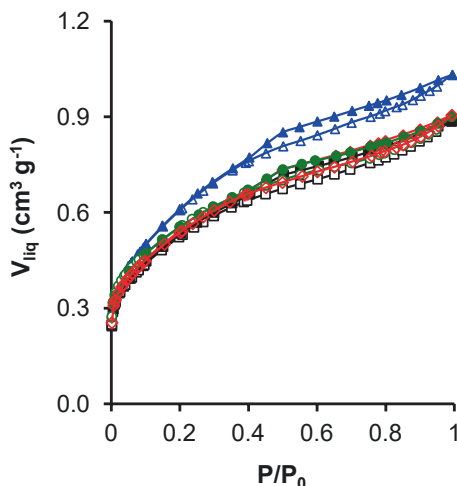


Table 13.1 Textural properties of activated carbon without functionalization (AC), activated carbon functionalized with melamine (AC-N), activated carbon functionalized with phosphoric acid (AC-P), and activated carbon functionalized with ammonium phosphate (AC-NP)

Sample	S_{BET} m ² /g	V_{micro} cm ³ /g	L_{micro} nm	V_{meso} cm ³ /g	L_{meso} nm	V_{macro} cm ³ /g	V_{T} cm ³ /g
AC	1224	0.442	1.33	0.375	2.46	0.145	0.962
AC-N	1169	0.420	1.36	0.404	2.44	0.125	0.951
AC-P	1296	0.450	1.37	0.484	2.38	0.123	1.071
AC-NP	1139	0.409	1.34	0.403	2.18	0.041	0.848

micropore mean width was centered on L_0 (N₂) 1.34 ± 0.03 nm, and mesopore mean width was centered on d , 2.36 ± 0.28 nm for AC materials, and this region represents the 80% of total area. These results agree with those reported by Moreno-Castilla et al. [13].

In addition to the available porous space, the surface chemistry of the material is essential for the stabilization of the adsorptive couple. The chemical compositions of the carbons are summarized in Table 13.2. In general, the surface of the materials was constituted mainly of C atoms ($\approx 80\%$) and presented residual nitrogen in AC-N and AC-NP for the functionalization method and phosphorus atoms either by the process of functionalization or activation. The pH_{IEP} becomes an important parameter to characterize the chemistry of carbons [29, 30]. It is defined as the pH value at which the total charge on the surface of the adsorbent is neutral [30] and determines the charge density of materials under different pH. Furthermore, it is strongly dependent on the chemical groups that possess the materials on their surfaces. The pH_{IEP} for all materials is acidic.

The use of the activating agent (H₃PO₄) promoted the formation of cross-links with phosphoryl groups; these chemical groups are proton-active and generate a negatively charged surface with low pH_{IEP} . Comparable results have been found by

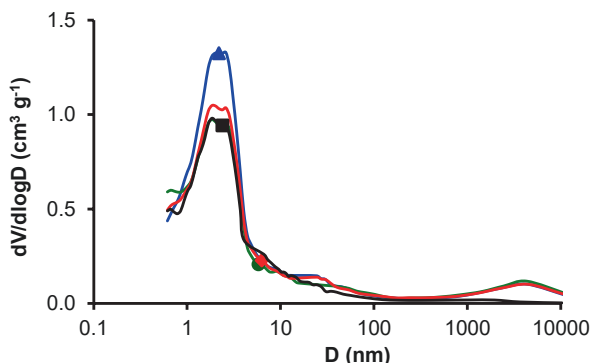


Fig. 13.3 Pore size distribution for: ●, activated carbon without functionalization (AC); ◆, activated carbon functionalized with melamine (AC-N); ▲, activated carbon functionalized with phosphoric acid (AC-P); and ■, activated carbon functionalized with ammonium phosphate (AC-NP). Obtained by the application of QSDFT to N_2 adsorption isotherms and mercury porosimetry

Table 13.2 Atomic concentration on the surface of activated carbon series. Assessed by XPS analysis

Sample	Surface atomic concentrations (%)					pH_{IEP}
	C1s	O1s	N1s	P2p	Heteroatoms (O + P)	
AC	85.5	7.7	–	6.7	14.4	2.44
AC-N	84.6	7.6	1.1	6.7	14.3	2.96
AC-P	83.4	7.7	–	8.9	16.6	1.92
AC-NP	82.3	7.7	0.6	7.3	15.0	2.03

other researchers [30]. The addition of heteroatoms such as nitrogen, free (N), or combined (NP), slightly increased the value of pH_{IEP} . However, for all AC materials, the surface chemistry is determined to a greater extent by the activating agent (H_3PO_4) [13, 31, 32]. In brief, the AC-N and AC-NP samples display a higher pH_{IEP} value than the other materials for the presence of amino groups on its surface (groups positively charged – Lewis bases). In contrast, AC and AC-P materials show the lowest value for pH_{IEP} due to the presence of phosphoryl groups, also called acid groups or proton-active that gives a negative charge density to the materials and, consequently, a lower value of pH_{IEP} [33].

13.3.2 Material Selection

The capacity of activated carbons with different chemical natures to remove uranyl was evaluated. Explicitly, the carbons evaluated reached removals of uranyl between 50% and 100% after 4 h. The adsorption efficiencies are given in the following order (97%) AC-N > (96%) AC > (81%) AC-NP > (56%) AC-P for the uranyl

concentration evaluated at temperature of 25 °C and adsorbent/adsorbate ratio of 10:1. Figure 13.4 shows the correlation between the porous and chemical properties of the materials and the ability to remove uranyl ions. According to the results, the mesoporous volume and the surface chemistry of the materials, measured through the pH_{IEP} and the heteroatoms (HETAM) content, are fundamental during the adsorption phenomenon (a high Pearson correlation coefficient (PCC) > 0.80). The macro- and microporous properties seem to have no relation with (PCC < 0.50) the adsorptive capacity of the materials on the uranyl ions.

In the present study, the correlation between the microporous volume and the adsorptive capacity of the materials seems not to be clear. However, the mesoporous carbons with the lowest number of heteroatoms (P + O), represented by a higher value for pH_{IEP} , were more efficient in the adsorption of uranyl. According to previous reports, uranyl chemical species at pH 6.3 are solvated with hydroxyl groups

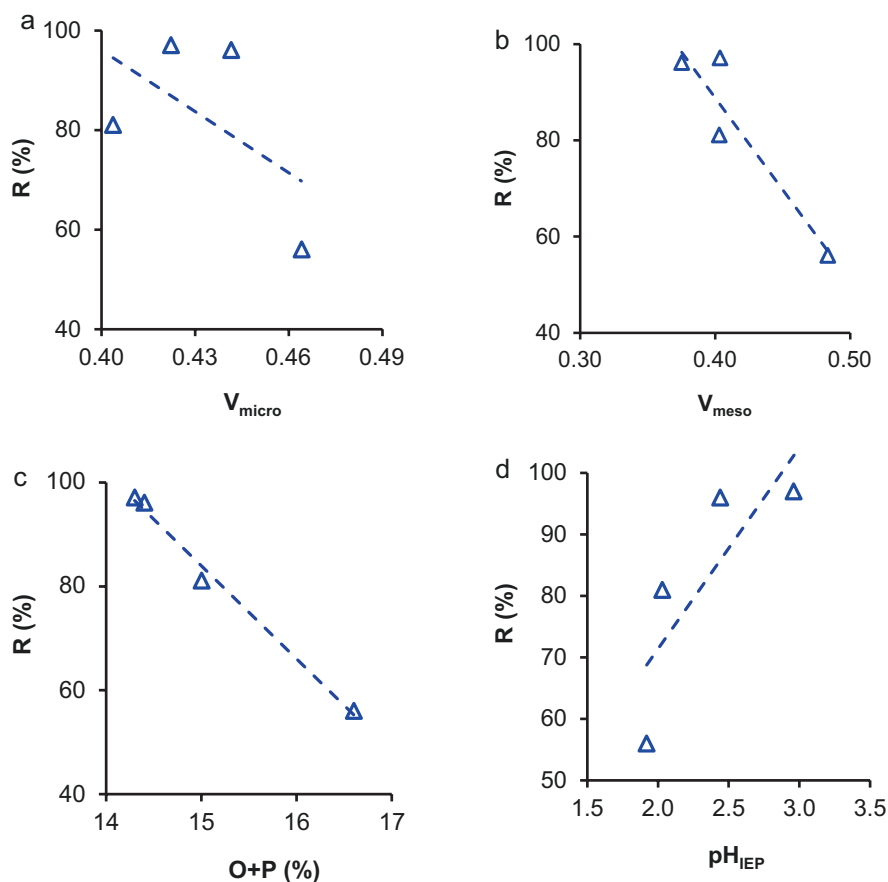


Fig. 13.4 Correlation between porous texture and chemical properties of materials and the ability to remove uranyl ions (R%)

associated with water molecules through ion-ion and ion-dipole interactions forming species like $\text{UO}_2(\text{OH})^+$, $(\text{UO}_2)_2(\text{OH})_2^{2+}$, and $(\text{UO}_2)_3(\text{OH})_5^+$ [34]; when the size and shape of a uranyl solvated with a single layer of water molecules are considered, as can be seen in Fig. 13.5, the inability of the complex to deposit correctly in the micropores (size <2 nm) is highlighted, unlike the narrow mesopores (slightly higher than 2 nm) that allow a better spatial accommodation of the hydrated uranyl.

On the other hand, less acidic surfaces, with higher pH_{IEP} benefited to a greater extent the uranyl – surface interaction. The high affinity between the adsorptive couple, Uranyl – AC, and Uranyl-AC-N, compared to the others materials it is due to a lower repulsive force between the highly electronegative zones of the complex attributed to the presence of oxygen atoms and the surface of the carbons AC and AC-N, less negative (higher pH_{IEP}). Materials such as AC-P and AC-NP are characterized by a more significant number of phosphoryl and phosphate groups (heteroatoms (P + O)), as can be seen in Table 13.2) that will eventually establish higher repulsive interactions with the uranyl group oxygen and decrease the adsorptive capacity of acid materials. Therefore, the most promising materials, AC and AC-N, were used for the adsorption efficiency tests.

13.3.3 Effect of Adsorbent/Adsorbate Ratio on the Adsorption Efficiency of Uranyl

Figure 13.6 shows the experimental isotherms for uranyl adsorption onto AC and AC-N materials with the BET model fit at 298 K using different adsorbent/adsorbate ratios. The adsorption isotherms for all scenarios have type III behavior according to the IUPAC classification [26]; in this type of isotherm, the adsorbate has a similar affinity for the adsorbent as for itself. The monolayer acts as a free site for another molecule to adsorb, and so on [25]; this leads to an uneven coating, with

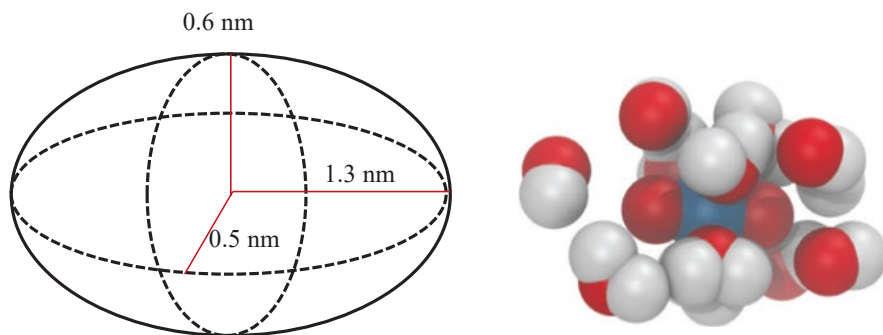


Fig. 13.5 Ellipsoid shape and mean size of a hydrated uranyl cation molecule with a single layer of water (five molecules) using dynamic

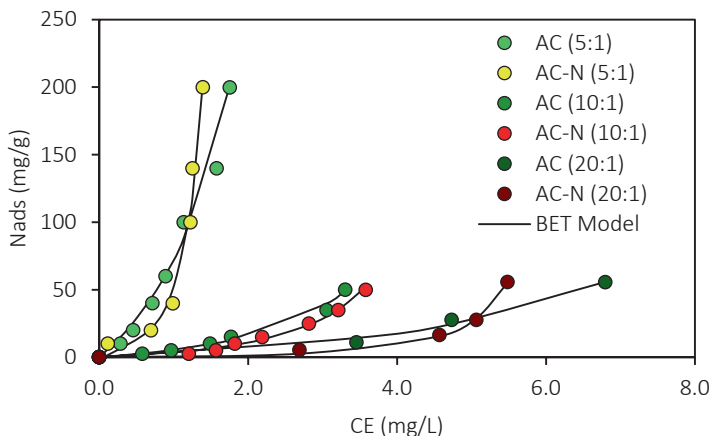


Fig. 13.6 Uranium-isotherms at 25 °C and different adsorbent/adsorbate ratio using activated carbon without functionalization (AC) ● 5:1, ● 10:1, ● 20:1 and activated carbon functionalized with melamine (AC-N) ● 5:1, ● 10:1, and ● 20:1

Table 13.3 Estimated BET model parameters for uranyl adsorption isotherms over activated carbon without functionalization (AC) and activated carbon functionalized with melamine (AC-N) using different adsorbent/adsorbate ratio

AC					AC-N				
<i>R</i>	<i>K_L</i> L/mg	<i>K_S</i> L/mg	<i>q_{max}</i> mg/g	<i>R</i> ²	<i>R</i>	<i>K_L</i> L/mg	<i>K_S</i> L/mg	<i>q_{max}</i> mg/g	<i>R</i> ²
5:1	0.35	0.14	200.8	0.97	5:1	0.53	0.06	200.58	0.98
10:1	0.18	0.07	58.2	0.99	10:1	0.18	0.05	55.64	0.99
20:1	0.09	0.04	54.9	0.99	20:1	0.15	0.02	51.14	0.99

free zones, other covered with monolayer, and parts covered with multilayer. These results agree with the report by other authors [15, 35].

There are no statistical differences between AC and AC-N during the uranyl adsorption. Moreover, as can be seen in Fig. 13.6, the isotherms showed a different amount of adsorbed according to the ratio adsorbate/adsorbent employed. The upper isotherm corresponds to 5:1, the middle isotherm to 10:1, and the lower isotherm to 20:1 adsorbent/adsorbate ratio, and the adsorbed amount decreases in the order 5:1 ratio > 10:1 ratio > 20:1 ratio in the entire range of equilibrium concentration (CE). These findings are supported by the values of BET model parameters listed in Table 13.3, where *q_{max}* decreases as the value of the ratio increases. Besides, *K_L* y *K_S* values followed a similar tendency of *q_{max}*, indicating that the adsorption affinity increases, and the multilayer adsorption greatly affected as the ratio adsorbate/adsorbent decreases for the two samples evaluated. As shown in Table 3, the BET model described well the experimental results of the adsorption isotherms according to the values of *R*². Lower *K_S* values related with increased ratio

adsorbate/adsorbent also indicate that adsorption is less stable and the uranyl molecules may be adsorbed perpendicularly to the carbon surface [22, 35, 36].

In this instance, the results can be attributed to the decrease of the available active sites for adsorption by mass units caused by increasing the carbon dosage, which consequently influences the interactions between the materials and uranyl. This condition improves carbon-carbon interaction and hence the diminution of the accessible active sites for adsorption. Therefore, this decreases the possibility of uranyl contacting the carbon surface. Similar results were published by Garcia et al. [35]. They assessed the adsorption of azo-dye Orange II over iron-benzene-tricarboxylate and observed a reduction in the amount adsorbed with the increase of the quantity of the adsorbent. Also, some authors like Guzman et al. [15] also found similar results when determining that the rise in the concentration of nanoparticles decreased the adsorbed amount of asphaltenes of them. In both studies, the results are attributed to the particle aggregation of adsorbent as a result of high adsorbent mass and the reduction of available porous sites. Finally, is important to remark that q_{\max} is mainly determined by the availability of sites on the materials, which decreases as amount of material increases.

13.3.4 Effect of Salinity on Adsorption Efficiency of Uranyl

When evaluating the impact of salinity on adsorption efficiency using AC and AC-N, 100% removal was evidenced at concentrations of uranyl between 50 and 1000 mg/L using saline concentrations of 1%, 3%, and 5% w/v, showing a higher performance in comparison with the non-saline system (uranyl removals between 56% and 97%). It appears that the presence of 1–5% w/v of saline concentration is enough to promote the total removal of uranyl, even when it is found at levels as diverse as 50 mg/L and 1000 mg/L. When AC and AC-N are at higher pHs than their pIIEP, negative sites on the material surfaces are favored. Thus, the probability of adsorbate-adsorbent encounter is reduced due to the high electronegativity of the uranyl molecules. The presence of ions in solution from the salt, especially the cations (M⁺), forms a bridge between the adsorptive pair establishing material (anion) – salt (cation) – uranyl (- dipole) interactions [37, 38].

13.3.5 Reuse Process of Activated Carbons

Reuse tests are useful to define the half-life time of absorbent materials. In the present study, 30 cycles of desorption-re-adsorption of uranyl on AC and AC-N materials were performed. The asequible sites of the carbons were restored by washing with 0.1 M NaOH, followed by de-ionized water and the subsequent sorption cycle. Thirty adsorption-desorption cycles were completed, and the adsorption power of AC and AC-N was found to be closely analogous during the 25th cycles. For the

AC-N, there is a decline by 15% in the 30th cycle, which can be due to the degradation of functionalizing agent. Meanwhile, the AC sample keeps constant during the 30 cycles evaluated. In addition, the results showed that desorption at basic pH is desirable for AC and AC-N recovery. These outcomes indicate that the activated carbons have a small affinity, rapidly saturable for some or all NaOH-modified uranyl species including uranyl hydroxide in the monomeric form $\text{UO}_2(\text{OH})_2$ and in the dimeric $(\text{UO}_2)_2(\text{OH})_4$ [34]. At pH 13, the AC and AC-N have a negative surface charge, and uranyl also tends to occur as an anionic species, for example, $\text{UO}_2(\text{OH})_2$ and $(\text{UO}_2)_2(\text{OH})_4$. This is an electrostatically unfavorable condition for the adsorption, which also can explain the decrease in the uranium adsorption on AC-N at pH 13 after 25 cycles. Currently, there is no knowledge of studies that report on the removal of uranyl species in fracturing waters; close research was done by Dutta et al. [34]; however, the assays were limited to interpreting the adsorptive phenomena in an aqueous medium; in that case, 93% or 186 mg/g removals of uranyl ions in the absence of salts at pH 6.0 were achieved. In comparison, in the present work, removals of 100% or 500 mg/g of uranyl ions at pH 6.3 and ranges of salinities between 0% and 5% were reached, which is one of the greatest adsorption efficacies described so far.

13.4 Conclusion

A new adsorbent made of activated carbon has been developed for fast and efficient adsorptive removal of uranyl ions at pH 6.3 as a proposal for water treatment in hydraulic fracturing processes. The results advised that the carbons with narrow mesoporosity and the highest value of pH_{IEP} were most efficient in the adsorption of uranyl, specifically AC and AC-N. The strong affinity is due to a lower repulsive force between the adsorptive couple added to the presence of narrow mesoporosity that allows the accommodation of hydrated uranyl species. On the other hand, the parameters of the BET model showed that the amount adsorbed decreases as the adsorbent/adsorbate ratio increases as a consequence of the reduction of available active sites for adsorption by mass unit, caused by increasing the carbon dosage and the aggregation of the primary particles of the material as previously reported. The BET adsorption isotherm suggested a maximum adsorption capacity (removal of %100) of 500 mg/g in 4 h, using a 5:1 of adsorbent/adsorbate ration and saline concentrations between 0% and 5% w/v which is a result not previously achieved since there is no knowledge of the removal of uranyl species from water used in hydraulic fracturing processes.

The sustainability of AC and AC-N has been demonstrated by showing the regeneration and reusability for 30 cycles. It is essential to highlight that the water used in hydraulic fracturing processes reports salinities and pHs in the ranges selected for the current investigation so that it can be concluded that AC and AC-N materials have tremendous potential for efficient uranium de-contamination of these waters. In future work, slight variations in pH could be considered on the removal capacity

of the investigated materials. Finally, it is presumed that the majority of NORM is found in anionic form, product of the combined action between the salts of the formation and the pH; therefore it would be correct to predict that the developed materials will be effective for the removal of other radioactive such as thorium and potassium.

Acknowledgments The authors would like to acknowledge Fondo Nacional de Financiamiento para la Ciencia, la Tecnología y la Innovación “Francisco José de Caldas,” Agencia Nacional de Hidrocarburos, Colciencias and Universidad Nacional de Colombia for their support provided in Agreement 064 of 2018 and Spanish Ministry of Science, Innovation and Universities - State Research Agency - Project ref. RTI2018-099224-B-I00. The authors also acknowledge Research Groups *Fenómenos de Superficie Michael Polanyi*, *Adsorción y Catálisis*, and especially to *Daniel Lopez Suarez* and *Ivan Moncayo* for their theoretical support in the research. Finally, authors thank Colciencias for the financing of the doctoral student Karol Zapata Acosta through the announcement 617/2014.

References

1. S. Zendejboudi, N. Rezaei, A. Lohi, Applications of hybrid models in chemical, petroleum, and energy systems: A systematic review. *Appl. Energy* **228**, 2539–2566 (2018)
2. Q. Wu, Y. Xu, X. Wang, T. Wang, S. Zhang, Volume fracturing technology of unconventional reservoirs: Connotation, design optimization and implementation. *Pet. Explor. Dev.* **39**, 377–384 (2012)
3. H. Wang, F. Ma, X. Tong, Z. Liu, X. Zhang, Z. Wu, D. Li, B. Wang, Y. Xie, L. Yang, Assessment of global unconventional oil and gas resources. *Pet. Explor. Dev.* **43**, 925–940 (2016)
4. J.D. Guzmán, D. Pineda, C.A. Franco, Ó.F. Botero, S.H. Lopera, F.B. Cortés, Effect of nanoparticle inclusion in fracturing fluids applied to tight gas-condensate reservoirs: Reduction of methanol loading and the associated formation damage. *J. Nat. Gas Sci. Eng.* **40**, 347–355 (2017)
5. M. Guo, X. Lu, C.P. Nielsen, M.B. McElroy, W. Shi, Y. Chen, Y. Xu, Prospects for shale gas production in China: Implications for water demand. *Renew. Sust. Energ. Rev.* **66**, 742–750 (2016)
6. G.V. Åkerblom, C. Wilson, Radon gas—A radiation hazard from radioactive bedrock and building materials. *Bull. Int. Assoc. Eng. Geol./Bull. l'Association Int. Géologie l'Ingénieur* **23**, 51–61 (1981)
7. A.W. Nelson, A.W. Knight, D. May, E.S. Eitheim, M.K. Schultz, Naturally-occurring radioactive materials (NORM) associated with unconventional drilling for shale gas, in *Hydraulic Fracturing: Environmental Issues*, ACS Symposium Series, vol. 1216, (American Chemical Society, Washington, DC, 2015), pp. 4–89. ISBN 9780841231221
8. T.A. Saleh, Naeemullah, M. Tuzen, A. Sari, Polyethylenimine modified activated carbon as novel magnetic adsorbent for the removal of uranium from aqueous solution. *Chem. Eng. Res. Des.* **117**, 218–227 (2017)
9. F. Khalili, G. Al-Banna, Adsorption of uranium(VI) and thorium(IV) by insolubilized humic acid from Ajloun soil – Jordan. *J. Environ. Radioact.* **146**, 16–26 (2015)
10. H. Ding, X. Luo, X. Zhang, H. Yang, Alginate-immobilized *Aspergillus niger*: Characterization and biosorption removal of thorium ions from radioactive wastewater. *Colloids Surf. A Physicochem. Eng. Asp.* **562**, 186–195 (2019)
11. S. Li, L. Wang, J. Peng, M. Zhai, W. Shi, Efficient thorium(IV) removal by two-dimensional Ti₂CTx MXene from aqueous solution. *Chem. Eng. J.* **366**, 192–199 (2019)

12. F.I. Khalili, N.H. Salameh, M.M. Shaybe, Sorption of uranium(VI) and thorium(IV) by Jordanian bentonite. *J. Chem.* **2013**, 586136 (2013)
13. C. Moreno-Castilla, F. Carrasco-Marín, M.V. López-Ramón, M.A. Alvarez-Merino, Chemical and physical activation of olive-mill waste water to produce activated carbons. *Carbon N. Y.* **39**, 1415–1420 (2001)
14. S. Eskandari, G. Tate, N.R. Leaphart, J.R. Regalbuto, Nanoparticle synthesis via electrostatic adsorption using incipient wetness impregnation. *ACS Catal.* **8**, 10383–10391 (2018)
15. J.D. Guzmán, S. Betancur, F. Carrasco-Marín, C.A. Franco, N.N. Nassar, F.B. Cortés, Importance of the adsorption method used for obtaining the nanoparticle dosage for Asphaltene-related treatments. *Energy Fuel* **2052–2059**, 30 (2016)
16. E. Bailón-García, F. Carrasco-Marín, A.F. Pérez-Cadenas, F.J. Maldonado-Hódar, Development of carbon xerogels as alternative Pt-supports for the selective hydrogenation of citral. *Catal. Commun.* **58**, 64–69 (2015)
17. A.F. Pérez-Cadenas, F.J. Maldonado-Hódar, C. Moreno-Castilla, On the nature of surface acid sites of chlorinated activated carbons. *Carbon N. Y.* **41**, 473–478 (2003)
18. C.A. Franco, N.N. Nassar, F.B. Cortés, Removal of oil from oil-in-saltwater emulsions by adsorption onto nano-alumina functionalized with petroleum vacuum residue. *J. Colloid Interface Sci.* **433**, 58–67 (2014)
19. S. Brunauer, P.H. Emmet, E. Teller. Adsorption of Gases in Multimolecular Layers. *J. Am. Chem. Soc.* **60**, 309–319 (1938)
20. A. Ebadi, J.S. Soltan Mohammadzadeh, A. Khudiev, What is the correct form of BET isotherm for modeling liquid phase adsorption? *Adsorption* **15**, 65–73 (2009)
21. A. Al-Futaisi, A. Jamrah, R. Al-Hanai, Aspects of cationic dye molecule adsorption to palygorskite. *Desalination* **214**, 327–342 (2007)
22. C.-H. Weng, Y.-F. Pan, Adsorption of a cationic dye (methylene blue) onto spent activated clay. *J. Hazard. Mater.* **144**, 355–362 (2007)
23. C.-H. Weng, Y.-F. Pan, Adsorption characteristics of methylene blue from aqueous solution by sludge ash. *Colloids Surf. A Physicochem. Eng. Asp.* **274**, 154–162 (2006)
24. K. Zapata Acosta, F. Carrasco-Marín, F. Cortés, C. Franco, S. Lopera, B. Rojano, Immobilization of *P. stutzeri* on activated carbons for degradation of hydrocarbons from oil-in-saltwater emulsions. *Nano* **9**, 500 (2019)
25. A. Elmouwahidi, Z. Zapata-Benabithé, F. Carrasco-Marín, C. Moreno-Castilla, Activated carbons from KOH-activation of argan (*Argania spinosa*) seed shells as supercapacitor electrodes. *Bioresour. Technol.* **111**, 185–190 (2012)
26. M. Thommes, K. Kaneko, A.V. Neimark, J.P. Olivier, F. Rodríguez-Reinoso, J. Rouquerol, K.S.W. Sing, Physisorption of gases, with special reference to the evaluation of surface area and pore size distribution (IUPAC technical report). *Pure Appl. Chem.* **87**, 1051–1069 (2015)
27. K. Zapata, F. Carrasco-Marín, J.P. Arias, J. Castelo-Quibén, C.A. Franco, B. Rojano, F.B. Cortés, Novel biomaterial design based on *Pseudomonas stutzeri*-carbon xerogel microspheres for hydrocarbon removal from oil-in-saltwater emulsions: A new proposed treatment of produced water in oilfields. *J. Water Process Eng.* **35**, 101222 (2020)
28. K. Zapata Acosta, F. Carrasco-Marín, F.B. Cortés, C.A. Franco, S.H. Lopera, B.A. Rojano, Immobilization of *P. stutzeri* on activated carbons for degradation of hydrocarbons from oil-in-saltwater emulsions. *Nanomater. Nanomater. (Basel)* **9**, 500 (2019)
29. P. Trivedi, L. Axe, Ni and Zn sorption to amorphous versus crystalline iron oxides: Macroscopic studies. *J. Colloid Interface Sci.* **244**, 221–229 (2001)
30. A. Lazaro, K. Sato, H.J.H. Brouwers, J.W. Geus, Pore structure development of silica particles below the isoelectric point. *Microporous Mesoporous Mater.* **267**, 257–264 (2018)
31. M. Tschapek, L. Tcheichvili, C. Wasowski, The point of zero charge (pzc) of kaolinite and SiO₂+Al₂O₃ mixtures. *Clay Miner.* **10**, 219–229 (1974)
32. M. Kosmulski, The pH-dependent surface charging and the points of zero charge. *J. Colloid Interface Sci.* **253**, 77–87 (2002)

33. M. Kosmulski, C. Saneluta, Point of zero charge/isoelectric point of exotic oxides: TiO_2 . *J. Colloid Interface Sci.* **280**, 544–545 (2004)
34. R.K. Dutta, M.A. Shaida, K. Singla, D. Das, Highly efficient adsorptive removal of uranyl ions by a novel graphene oxide reduced by adenosine 5'-monophosphate (RGO-AMP). *J. Mater. Chem. A* **7**, 664–678 (2019)
35. E.R. García, R.L. Medina, M.M. Lozano, I. Hernández Pérez, M.J. Valero, A.M.M. Franco, Adsorption of azo-dye orange II from aqueous solutions using a metal-organic framework material: Iron-benzenetricarboxylate. *Materials (Basel)* **7**, 8037–8057 (2014)
36. J. Wang, C.P. Huang, H.E. Allen, D.K. Cha, D.-W. Kim, Adsorption characteristics of dye onto sludge particulates. *J. Colloid Interface Sci.* **208**, 518–528 (1998)
37. B. Biswas, B. Sarkar, R. Rusmin, R. Naidu, Bioremediation of PAHs and VOCs: Advances in clay mineral-microbial interaction. *Environ. Int.* **85**, 168–181 (2015)
38. U.C. Ugochukwu, M.D. Jones, I.M. Head, D.A.C. Manning, C.I. Fialips, Biodegradation and adsorption of crude oil hydrocarbons supported on “homoionic” montmorillonite clay minerals. *Appl. Clay Sci.* **87**, 81–86 (2014)